

## A strengthened East Asian Summer Monsoon during Pliocene warmth: Evidence from ‘red clay’ sediments at Pianguan, northern China

Shiling Yang<sup>a,b,\*</sup>, Zhongli Ding<sup>a,b</sup>, Shaohua Feng<sup>c</sup>, Wenying Jiang<sup>a</sup>, Xiaofang Huang<sup>a,b</sup>, Licheng Guo<sup>a,b</sup>

<sup>a</sup> Key Laboratory of Cenozoic Geology and Environment, Institute of Geology and Geophysics, Chinese Academy of Sciences, Beijing 100029, China

<sup>b</sup> University of Chinese Academy of Sciences, Beijing 100049, China

<sup>c</sup> Beijing Geotechnical and Investigation Engineering Institute, Beijing 100083, China



### ARTICLE INFO

#### Keywords:

Red clay  
Loess  
Paleosol  
Paleomagnetism  
East Asian Summer Monsoon  
Pliocene warmth

### ABSTRACT

The Pliocene epoch (5.3–2.6 Ma) is the most recent geological interval in which atmospheric CO<sub>2</sub> levels were similar to those of the present day (~400 ppmv). This epoch is therefore considered to be the best ancient analog for predicting a future anthropogenic greenhouse world. In order to determine the response of the East Asian Summer Monsoon (EASM) rainbelt during Pliocene warmth, a 71.9 m-thick aeolian ‘red clay’ sequence at Pianguan was investigated. Rock magnetic experiments suggest that magnetite of pseudo-single domain size is the dominant remanence carrier in the ‘red clay’ sequence. Magnetostratigraphic data, constrained by lithostratigraphy, show that the polarity zones of the ‘red clay’ section correlate with those between subchrons C2An.2r and C3An.2n of the geomagnetic polarity time scale (GPTS), yielding an age range of 6.9–2.9 Ma. The ‘red clay’ deposits exhibit enhanced weathering intensity over two time intervals, namely 5.23–4.3 Ma and 3.7–2.9 Ma, as evidenced by their well-developed pedogenic characteristics, as well as their high free to total Fe<sub>2</sub>O<sub>3</sub> ratios and high redness (a\*) values, which in turn indicate an increased summer monsoon intensity during most of the Pliocene. Furthermore, the pedogenic characteristics of the well-weathered Pliocene soils were compared with those of paleosol unit S<sub>5</sub> (one of the best-developed soil units found in Pleistocene loess) from the Yulin, Luochuan and Lantian sections, which constitute a north-south transect across the Chinese Loess Plateau (CLP). The Pliocene soils at Pianguan show a pedogenic development similar to the S<sub>5</sub> (~0.5 Ma) at Luochuan in the central Plateau, which is located some 3.7° latitude south of Pianguan, but this development is much stronger than that observed at Yulin in the north, and weaker than that seen at Lantian in the south. This may imply a more northerly penetration (~400 km) of the monsoon rainbelt during Pliocene warmth compared with the Pleistocene interglacial period (~0.5 Ma ago), supporting the prediction that the EASM rainbelt shifts northward in a warmer world. In addition, our results show that Pliocene warmth was unlikely to have been characterized by a permanent El Niño-like state, but was possibly influenced by a La Niña-like state.

### 1. Introduction

The East Asian Summer Monsoon (EASM) is an important component of global-scale atmospheric circulation, and as such plays a key role in heat and moisture transport from low- to mid-latitudes (Webster et al., 1998; Ding, 2004), and even to high-latitudes (Ploeger et al., 2013). Variations in the position and intensity of the summer monsoon often cause devastating floods or droughts in densely populated East Asia. In recent years, the response of the summer monsoon to a CO<sub>2</sub>-induced warmer climate has become the subject of increasing concern. Hydroclimatic changes in East Asia from the Last Glacial Maximum (LGM) to the Holocene have been investigated to evaluate the

significance of the current warming trend (Quade and Broecker, 2009; Yang et al., 2015a). However, a striking difference between the LGM to Holocene warming and the current global warming is that during the former, atmospheric CO<sub>2</sub> levels increased slowly from ~180 to ~260 ppmv (Lüthi et al., 2008), whereas they have risen rapidly from ~280 ppmv in pre-industrial times (Etheridge et al., 1996) to over 400 ppmv today, and are projected to rise further in the next few decades as fossil fuels continue to be exploited (IPCC, 2013; Rogelj et al., 2016). As today's climate is far out of equilibrium with these elevated CO<sub>2</sub> levels because of the large thermal inertia of the oceans (Levitus et al., 2000; Back et al., 2013), an investigation into the equilibrium hydroclimatic response in East Asia has great practical

\* Corresponding author at: Key Laboratory of Cenozoic Geology and Environment, Institute of Geology and Geophysics, Chinese Academy of Sciences, Beijing 100029, China.  
E-mail address: [yangsl@mail.iggcas.ac.cn](mailto:yangsl@mail.iggcas.ac.cn) (S. Yang).

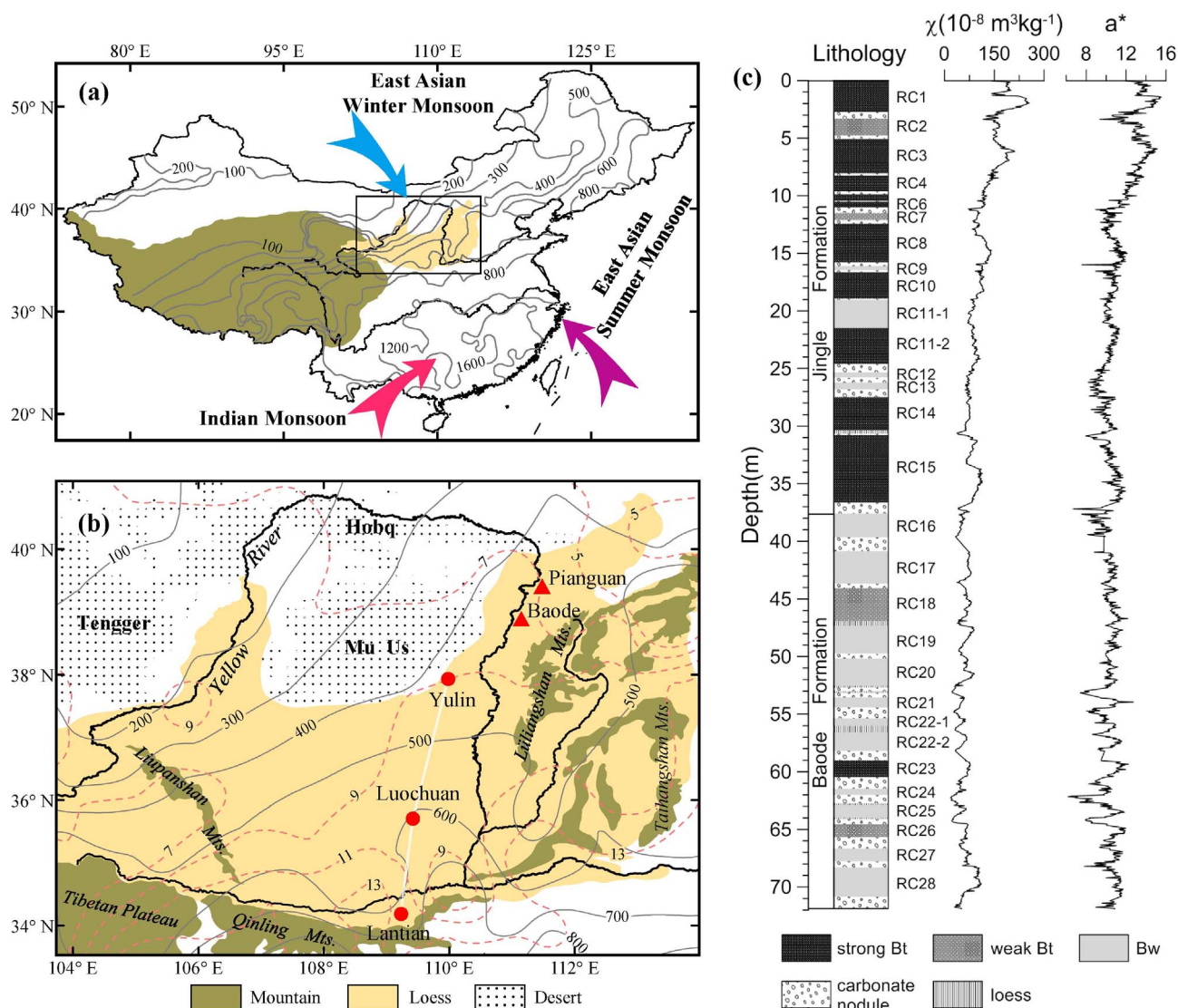


**Fig. 1.** (a) Prevailing monsoonal circulation (arrows) and modern mean annual precipitation distribution in China. (b) Study sites and modern climatic gradients on the Chinese Loess Plateau. The isohyets (mm; grey lines) and isotherms (°C; dashed lines) are values averaged over 51 years (1951–2001). The white line indicates the north-south Pleistocene paleosol (S<sub>5</sub>) transect consisting of three sections (Yulin, Luochuan and Lantian). (c) Stratigraphic column, magnetic susceptibility ( $\chi$ ), and redness ( $a^*$ ) for the Pianguan 'red clay' sequence.

significance for humankind.

The Pliocene epoch (5.3–2.6 Ma) is the most recent geological interval which experienced atmospheric CO<sub>2</sub> levels of ~400 ppmv (Pagani et al., 2010; Seki et al., 2010; Bartoli et al., 2011; Beerling and Royer, 2011). During this epoch, global mean annual surface temperatures were 2.7–4.0 °C warmer than pre-industrial values (Pagani et al., 2010; Haywood et al., 2013, 2016), and continental configurations and ocean bathymetries were similar to the present day (Dowsett et al., 2010). Therefore, the Pliocene is often considered the best ancient analog for predicting future climate scenarios (Mohtadi et al., 2016).

Aeolian 'red clay' on the Chinese Loess Plateau (CLP) holds a valuable archive of the East Asian Monsoon during the Neogene (Ding et al., 1999, 2001a; An, 2000; Yang and Ding, 2004, 2010). Previous studies have shown a southerly increase in weathering intensity for both the Pliocene 'red clay' (Han et al., 2007) and the Pleistocene interglacial paleosols (Yang and Ding, 2003), indicating a spatial climatic pattern similar to the present day, i.e. a north-south increasing trend of temperature and rainfall (Fig. 1a and b) during the Plio-Pleistocene. However, the north-south climatic gradient might be flatter during the Pliocene than during Pleistocene interglacials (Han et al., 2007).

Geographically, the northern CLP is located in the marginal zone of the EASM, and so sites in the northern CLP or farther north are more sensitive to the advance or retreat of the monsoonal rainbelt, and are thus crucial for any investigations into the hydroclimatic regime in existence during periods of Pliocene warmth.

Recently, we found a new 'red clay' section in the northernmost CLP. In this study, we first present magnetostratigraphic results for this section, then quantify its weathering intensity by color and Fe<sub>2</sub>O<sub>3</sub> content analysis, and finally compare its pedogenic characteristics with those of a representative interglacial paleosol within Pleistocene loess, with the aim of addressing the monsoonal rainbelt shift during Pliocene warmth.

## 2. Setting and stratigraphy

On the CLP, there is a set of reddish Neogene clay-silt deposits beneath the Quaternary loess, which were initially known as "Hippurion clay" (Andersson, 1923; Zdansky, 1923; Teilhard de Chardin and Young, 1930) as they commonly contain *Hippurion* fossils. In the 1980s, Tungsheng Liu and his coworkers informally named these sediments 'red clay' (Liu, 1985), a label which has been widely used ever since.

The section we studied is located at Pianguan (39.42°N, 111.48°E; Fig. 1b), ~110 km northeast of the eastern margin of Mu Us Desert. At present, the mean annual temperature and precipitation at Pianguan are about 7 °C and 420 mm, respectively. The section is 71.9 m thick, underlain conformably by alluvial silt with sparse fine gravels, and overlain with an angular unconformity by late Pleistocene loess. Like other ‘red clay’ sections on the CLP (Ding et al., 1998a, 1999, 2001b; Zhu et al., 2008; Anwar et al., 2015), the most striking features of the ‘red clay’ sequence at Pianguan are its reddish color and the alternation of soils (0.3–5.75 m thick) and carbonate nodule layers (0.15–1.3 m thick) (Fig. 1c). The soils generally have a subangular blocky structure and few to many translocated clay skins and/or dark Fe–Mn films, and thus can be designated as B horizons. Based on its pedogenic morphology, these B horizons can be classified into three types: Bw; weak Bt; and strong Bt. The Bw horizons generally have a weak, coarse subangular blocky structure without, or with only a few, clay skins. The weak Bt horizons are characterized by a moderate, medium subangular blocky structure and few, to common, translocated clay skins and/or Fe–Mn films. The strong Bt horizons have a strong, fine subangular structure and many clay skins and/or Fe–Mn films. In general, the upper and lower boundaries of the B horizons are indistinct, and pedogenic A horizons are lacking. In this study, we used an RCi system to label the ‘red clay’ sequence, and a total of 28 couplets of soils and carbonate nodule horizons were observed. An RC unit contained one or more soil B horizons.

From a lithostratigraphic point of view, the ‘red clay’ strata in northern China consists of two formations from base to top: the Baode Formation and the Jingle Formation. Although stratigraphic and paleontological studies began as early as the 1920–1930s (Zdansky, 1923; Teilhard de Chardin and Young, 1930), an accurate age range for the Jingle Formation was only recently determined to be 5.34–2.72 Ma in the Baode ‘red clay’ section (Fig. 1b; Zhu et al., 2008). At Baode, the Jingle Formation has pedogenic characteristics more advanced than in the Baode Formation, as suggested by its much redder color and more, and thicker, clay skins and Fe–Mn films (Zhu et al., 2008). Based on a stratigraphic correlation between the Pianguan and Baode sections, the boundary between the Jingle and Baode Formations is readily identified in the Pianguan ‘red clay’ sequence. The soils from 0 m to 37.7 m depth (RC1–RC15) are grouped into the Jingle Formation (Fig. 1c), while those between 37.7 m and 71.9 m depth (RC16–RC28) are assigned to the Baode Formation. The soils in the Jingle Formation mostly have strong Bt horizons, while those in the Baode Formation generally have Bw or weak Bt horizons. The Jingle Formation shows higher magnetic susceptibility ( $\chi$ ) and redness ( $a^*$ ) values than the Baode Formation (Fig. 1c). In addition, seven typical loess units, varying in thickness from 0.15 m to 0.9 m, are observed in the Baode Formation.

In addition to the ‘red clay’ sequence, the paleosol unit  $S_5$  (~0.5 Ma), one of the best-developed soils in Chinese loess, was studied at the Yulin (37.94°N, 109.98°E), Luochuan (35.71°N, 109.42°E) and Lantian (34.24°N, 109.12°E) sections along a north-south transect (Fig. 1b). At present, the mean annual temperature at Yulin is 9 °C, and the mean annual precipitation is 410 mm; the values for Lantian are 13 °C and ~600–650 mm, respectively. The  $S_5$  soil unit shows a southward increase in pedogenic development along the transect, similar to the pattern of the present day north-south climatic gradient.

### 3. Methods

At Pianguan, 1349 samples were taken at 5 cm intervals for magnetic susceptibility and color reflectance measurements. Three hundred forty-eight oriented block samples were collected at intervals of 20–30 cm for paleomagnetic analysis. For the north-south soil unit ( $S_5$ ) transect, 529 samples were taken at intervals of 5 cm. Low-field magnetic susceptibility ( $\chi$ ) and color reflectance were measured on all samples using a Bartington Instruments MS2 magnetic susceptibility meter and a Minolta-CM2002 spectrophotometer. The color reflectance

of all samples was quantified using the spherical  $L^*a^*b^*$  color space. We used red-green chromaticity  $a^*$  ( $+a^*$  is the red direction,  $-a^*$  is the green direction) to characterize the ‘red clay’ sequence (Fig. 1c). The color reflectance analytical procedures used were as detailed by Yang and Ding (2003). The ratio of citrate–bicarbonate–dithionite (CBD)–extractable  $Fe_2O_3$  (free  $Fe_2O_3$ ) to total  $Fe_2O_3$  concentrations was measured for 208 samples. Free  $Fe_2O_3$  was extracted using the CBD method (Mehra and Jackson, 1960). The samples for total  $Fe_2O_3$  concentration determination were dissolved with an HF–HClO<sub>4</sub>–HNO<sub>3</sub> mixed solution. Both the free and total iron concentrations were measured using a GGX-600 atomic absorption spectrophotometer. Analytical uncertainties were  $\pm 5\%$  for both free and total  $Fe_2O_3$  content.

Before conducting thermal demagnetization, rock magnetic experiments, including measurements of temperature-dependent susceptibility ( $\chi$ –T curves), the hysteresis loop, and isothermal remanent magnetization (IRM) and its back-field demagnetization characteristics, were performed on representative samples to identify magnetic remanence carriers.  $\chi$ –T curves were measured using an MFK1-FA Kappabridge instrument equipped with a CS-4 high-temperature furnace able to heat samples from room temperature to 700 °C in an argon atmosphere. Hysteresis loops and IRM acquisition curves and their backfield demagnetization characteristics were measured at room temperature using a MicroMag 3900 Vibrating Sample Magnetometer. Finally, progressive thermal demagnetization (14–17 steps) was performed on all the oriented specimens from room temperature to 610 °C or 675 °C at 20–50 °C intervals, using a MMTD80 Thermal Demagnetizer. All remanences were measured using a 2G Enterprises Model 760-R cryogenic magnetometer installed in a magnetically shielded room (< 300 nT).

### 4. Magnetic carrier mineral

For all the selected samples, the magnetic susceptibility increases gradually from room temperature to ~200–250 °C (Fig. 2a), which can be interpreted as a result of the gradual unblocking of fine-grained single domain (SD) ferrimagnetic particles (Liu et al., 2005). From ~250 to 450 °C, the susceptibility decreases gradually (Fig. 2a), which may be attributed to the conversion of metastable maghemite to hematite (Stacey and Banerjee, 1974; Liu et al., 1999, 2005). All the heating curves are characterized by a distinct decrease in magnetic susceptibility towards ~580 °C (Fig. 2a), the Curie point of magnetite, indicating the major contribution made by magnetite to the magnetic susceptibility. For each sample, the cooling curve is lower by varying degrees than the heating curve (Fig. 2a), likely due to the production of weakly magnetic hematite during thermal treatment (Heller et al., 1991; Liu et al., 2010).

The hysteresis loops close above 300 mT (Fig. 2b), which is characteristic of the dominant ferrimagnetic phase. All the samples show a rapid increase in IRM acquisition below 100 mT (Fig. 2c), and an acquired 91–97% of the saturation isothermal remanent magnetization (SIRM) in a field of 300 mT. Results of the back-field IRM demagnetization (Fig. 2c) show low coercivity of remanence ( $B_{cr}$ ) values (< 33 mT). The S-ratio provides a measure of the relative contribution of low- and high-coercivity material to the SIRM (Stober and Thompson, 1979; Bloemendal et al., 1992; Maxbauer et al., 2016). The S-ratio values of all the samples are close to 1 (Fig. 2c), indicating a major contribution of low-coercivity magnetic minerals such as magnetite and/or maghemite. Results of the hysteresis loops and IRM measurements, along with the  $\chi$ –T curves, unambiguously suggest that magnetite is the dominant remanence carrier in the ‘red clay’ sequence, which is consistent with the results from other ‘red clay’ sections on the CLP (Liu et al., 2001; Qiang et al., 2005).

In addition, saturation magnetization ( $M_s$ ), saturation remanence ( $M_{rs}$ ), coercivity ( $B_c$ ), and coercivity of remanence ( $B_{cr}$ ) values were determined and their ratios plotted on a ‘Day plot’ of  $M_{rs}/M_s$  versus  $B_{cr}/B_c$  (Day et al., 1977; Dunlop, 2002) to determine the domain state of

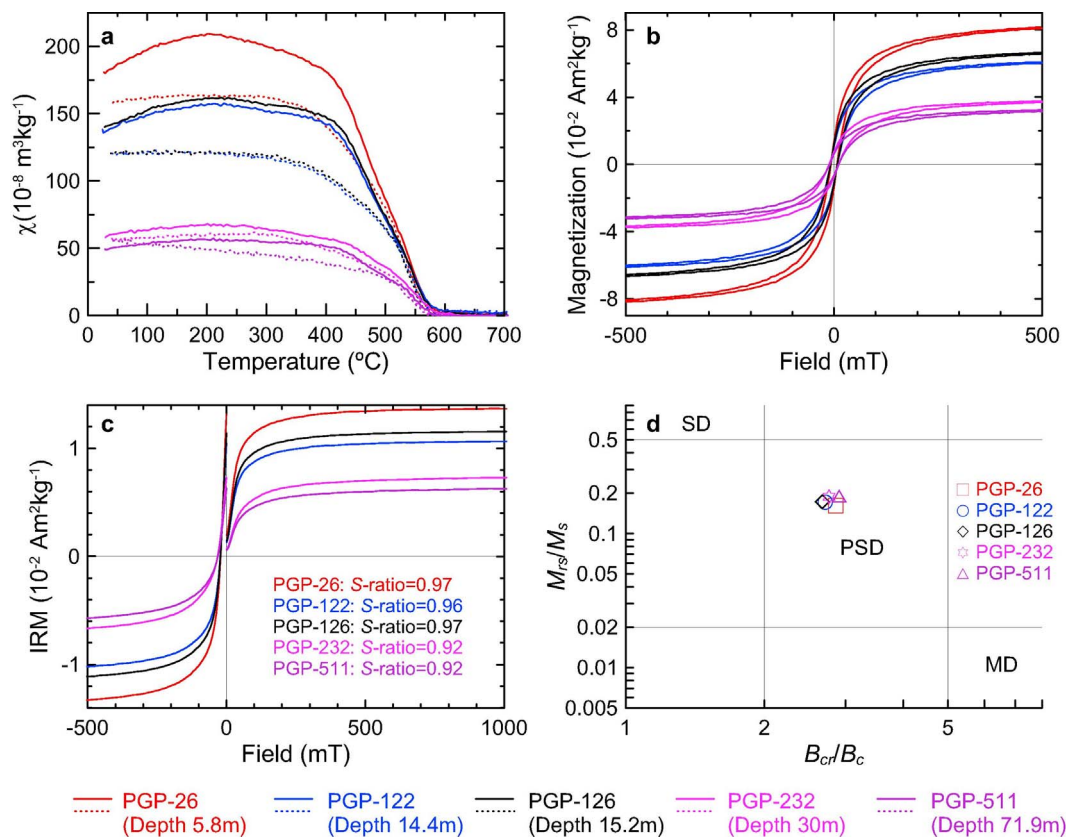


Fig. 2. Rock magnetic results for five representative 'red clay' samples from the Pianguan section. (a) Temperature-dependent magnetic susceptibility ( $\chi$ -T) curves. Solid (dotted) lines indicate heating (cooling) curves. (b) Hysteresis loops after paramagnetic slope correction. (c) Acquisition of isothermal remanent magnetization (IRM) and back-field demagnetization of the saturation isothermal remanent magnetization (SIRM). SIRM is defined here as the IRM acquired in a magnetic field of 1.0 T.  $S$ -ratio =  $0.5 \times [(-\text{IRM}_{-300\text{mT}}/\text{SIRM}) + 1]$  (Bloemendal et al., 1992). (d) 'Day plot' with SD (single domain), PSD (pseudo-single domain), and MD (multi-domain) zonations, after Dunlop (2002).

magnetite in the samples (Fig. 2d). All data cluster closely within the pseudo-single domain (PSD) field, showing a similar grain size of magnetite throughout the 'red clay' sequence.

## 5. Magnetostratigraphy

Orthogonal projections of vector end-points for progressive thermal demagnetization (Zijderveld, 1967) show that the measured natural remanent magnetization (NRM) is characterized by two magnetic components (Fig. 3). The low temperature component ( $< 300^{\circ}\text{C}$ ) has a direction consistent with the present geomagnetic field, and is commonly considered to be a viscous remanent magnetization in aeolian deposits (Heller and Liu, 1982; Ding et al., 2001b). Between 300 and  $550^{\circ}\text{C}$ , a stable component is observed (Fig. 3), and is interpreted as a characteristic remanent magnetization (ChRM). ChRM directions were calculated using a principal component analysis (Kirschvink, 1980). A total of 303 (87%) samples with a maximum angular deviation (MAD) of  $< 15^{\circ}$  yielded well-defined ChRM directions (Fig. 4). Virtual geomagnetic pole (VGP) latitudes from the ChRM vectors were used to develop a magnetic polarity stratigraphy (Fig. 4), which consists of 16 polarity intervals.

In complete loess-'red clay' sequences on the CLP, the Gauss/Matuyama geomagnetic reversal (2.58 Ma) has been found to occur uniformly around the 'red clay'-loess contact zone (Heller and Liu, 1984; Liu, 1985; Rutter et al., 1990; Zheng et al., 1992; Sun et al., 1998; Ding et al., 1998a, 1998b, 2001b; Yang and Ding, 2010), thus providing an important age constraint for the magnetostratigraphy of the 'red clay'. In the Pianguan section, the Gauss/Matuyama reversal was not recorded because there is a lengthy hiatus between the 'red clay' and its overlying loess. Fortunately, the boundary between the Jingle and Baode Formations, recently dated to 5.34 Ma (around the C3n.4n-C3r

reversal) (Zhu et al., 2008), provides a critical age constraint for the correlation of the magnetic polarity stratigraphy to the geomagnetic polarity time scale (GPTS) (Fig. 4). In the Pianguan section, a geomagnetic reversal is observed at exactly the base of the Jingle Formation (37.5 m depth; Fig. 4), which can be defined as the base of subchron C3n.4n. Thus the five reverse magnetozones from a depth of 29.5 m upward to 2.9 m within the Jingle Formation are correlated to C3n.3r, C3n.2r, C3n.1r, C2Ar, and C2An.2r. The polarity of the uppermost 2 m of 'red clay' is not interpreted, because it is characterized by low VGP latitudes, which may be a result of subsequent disturbance due to erosion, as evidenced by its overlying angular unconformity. The two normal magnetozones between 44.9 m and 68 m within the Baode Formation are interpreted as C3An.1n and C3An.2n. The reverse magnetozone in the lowermost 3.9 m may represent part of C3Ar chron.

The above magnetic polarity interpretation yields two linear regressions of age versus depth for the 'red clay' sequence (Fig. 5). One is for the lower part of the sequence (6.7–4.3 Ma), which has an average sedimentation rate of 22.47 m/Ma, and the other is for the upper part (4.3–3.2 Ma), with an average sedimentation rate of 9.58 m/Ma. Using linear extrapolation of the sedimentation rates, we estimated an age of 6.9 Ma and 2.9 Ma for the base and top of the section, respectively.

## 6. East Asian Summer Monsoon during Pliocene warmth

### 6.1. Changes in summer monsoon intensity from 6.9 to 2.9 Ma

The magnetic susceptibility and redness ( $a^*$ ) show a similar variation pattern in the Pianguan section (Fig. 6). From 6.9 to 5.23 Ma, the magnetic susceptibility and redness oscillate stably in the range  $15\text{--}110 \times 10^{-8} \text{ m}^3 \text{ kg}^{-1}$  and 8–12, respectively, while they exhibit an oscillatory increase from 5.23 Ma to 2.9 Ma, and reach as high as

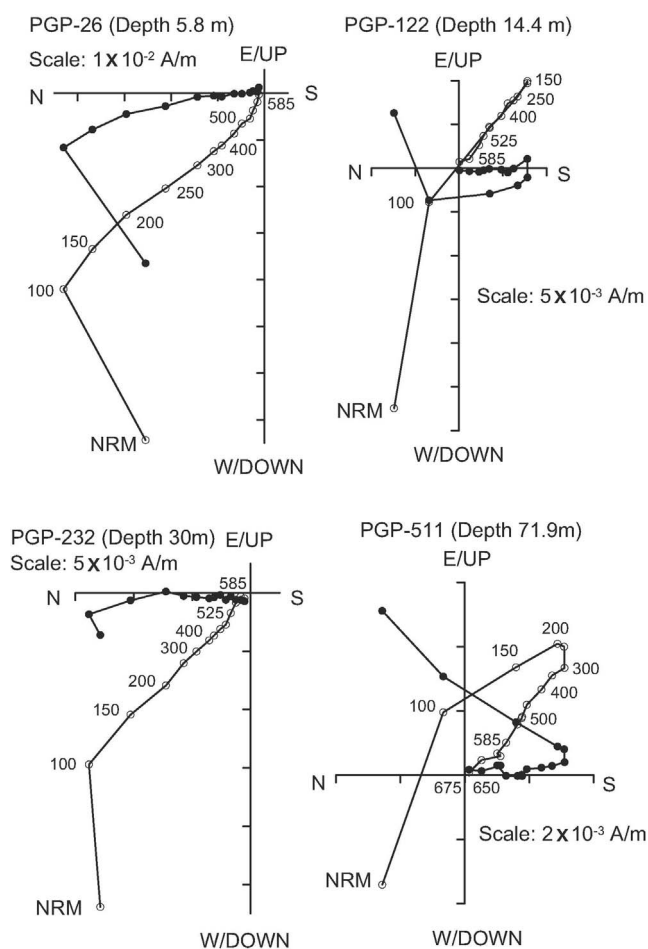


Fig. 3. Orthogonal projections of progressive thermal demagnetization of natural remanent magnetization (NRM) for four representative specimens from the Pianguan section. Solid (open) circles represent projections onto the horizontal (vertical) plane. Thermal demagnetization temperatures are indicated in °C.

$250 \times 10^{-8} \text{ m}^3 \text{ kg}^{-1}$  for the susceptibility and 15.5 for the redness at  $\sim 3.1$  Ma. For the iron record, high free to total  $\text{Fe}_2\text{O}_3$  ratios (up to 0.37) are observed during two major time intervals, i.e. 5.23–4.3 Ma and 3.7–2.9 Ma, while relatively low  $\text{Fe}_2\text{O}_3$  ratios occur during the intervals 6.9–5.23 Ma and 4.3–3.7 Ma.

Previous studies have shown that magnetic susceptibility, the widely used paleomonsoonal proxy for loess deposits, is not applicable to the ‘red clay’ (Ding et al., 2001a), because well-developed soils in ‘red clay’ always exhibit low magnetic susceptibility values as a result of substantial gleying under a reduced environment. Instead, the ratio of free to total  $\text{Fe}_2\text{O}_3$  has been demonstrated to be basically controlled by weathering intensity changes, and is thus a useful proxy for paleomonsoonal reconstruction (Ding et al., 2001a). In the Pianguan section, although the magnetic susceptibility displays a variation pattern similar to the color record (Fig. 6), its paleoclimatic interpretation remains to be clarified. The  $\text{Fe}_2\text{O}_3$  ratio record, as well as the redness ( $a^*$ ) record, depicts two strongly weathered portions of the ‘red clay’ (RC1–RC4 and RC8–RC15) within the Jingle Formation (Fig. 6), consistent with their well-developed soil characteristics. All this evidence suggests a strengthened EASM during the intervals 5.23–4.3 Ma and 3.7–2.9 Ma.

## 6.2. Shifting of the East Asian monsoonal rainbelt during Pliocene warmth

The occurrence of strongly developed Pliocene soils in the northern CLP allows us to evaluate the shift in the monsoonal rainbelt by virtue of a comparison between the pedogenic intensity of the ‘red clay’ and Pleistocene paleosols. On the CLP, the  $S_5$  paleosol is one of the best-

developed soils within the loess-soil sequence, and as such serves as a prominent stratigraphic marker (Liu, 1985; Ding et al., 1993, 1999). It consists of three individual soils ( $S_{5-1}$ ,  $S_{5-2}$ , and  $S_{5-3}$ ; Fig. 7) showing a better-developed pedogenic structure, higher magnetic susceptibility and redness ( $a^*$ ) values than are found in most other soils.  $S_{5-1}$  is the best developed unit in the  $S_5$  soil complex, and was thus selected for comparison.

At Yulin, on the northern CLP, the  $S_{5-1}$  unit has Bw horizons with a weak, coarse subangular blocky structure without clay skins or Fe–Mn films (Fig. 8a). In the Luochuan section on the central CLP, the  $S_{5-1}$  unit exhibits Bt horizons with a strong, fine subangular structure, and many clay skins (Fig. 8b), with few Fe–Mn films. At the Lantian section on the southern CLP, the  $S_{5-1}$  unit displays Bt horizons with a strong, fine prismatic structure, many, thick clay skins (Fig. 8c), and numerous Fe–Mn films. From Yulin to Lantian along the north-south transect, the  $S_{5-1}$  unit shows a southward increase in its magnetic susceptibility and redness ( $a^*$ ) values (Fig. 7), which is in agreement with the southerly increase in the pedogenic development of the soil (Fig. 8a–c). The well-weathered Pliocene soils at Pianguan, such as RC1, RC3, RC8, RC14, and RC15, have a fine subangular structure and contain many clay skins (Fig. 8d–f) and some Fe–Mn films, showing a pedogenic development much stronger than that of  $S_{5-1}$  at Yulin on the northern CLP, but similar to Luochuan on the central CLP.

In general, the formation of clay skins is a result of the percolation of dilute clay suspension through soils under wet conditions, which commonly occurs between pH values of 4.5 and 6.5 when carbonate has been completely dissolved (Soil Survey Staff, 1999; Ding et al., 2001a). Therefore, the abundance of translocated clay skins within soil B horizons is regarded as the most important pedogenic characteristic in interpreting soil-forming climatic conditions (Ding et al., 1999, 2001a), with higher clay skin contents suggesting wetter climatic conditions, or a stronger summer monsoon.

The comparison of the ‘red clay’ and  $S_{5-1}$  unit indicates that the climatic conditions of the northernmost CLP during periods of Pliocene warmth may have been similar to those of the central CLP during a typical Pleistocene interglacial. As the Pianguan section is located some  $3.7^\circ$  latitude north of the Luochuan section, we thus inferred a  $\sim 400$  km northward migration of the monsoonal rainbelt during the Pliocene compared with the Pleistocene interglacial period ( $\sim 0.5$  Ma ago). The existence of a strengthened summer monsoon during Pliocene warmth is strongly supported by increased arboreal pollen in ‘red clay’ from both the northern (Li et al., 2011) and central CLP (Wu et al., 2007), relative to Pleistocene interglacial soils (Cai et al., 2013; Jiang et al., 2013, 2014; Yang et al., 2015b), and by a northward shift of the  $C_4$  vegetation maximum zone on the CLP (Passey et al., 2009). It should be noted that, except for monsoonal precipitation, other factors such as the time duration of soil development and geomorphological conditions could also have played a significant role in the development of pedogenic characteristics. The estimation of the migration distance for the monsoonal rainbelt therefore remains a preliminary one, and will be subject to future revision as more data become available.

## 6.3. Mechanisms

The response of the regional hydroclimate to future greenhouse warming has been much debated. As moisture content in the atmosphere rises with temperature (Trenberth et al., 2003), Held and Soden (2006) suggested that global warming will intensify the existing patterns of atmospheric moisture convergence and divergence, thereby increasing effective precipitation in humid regions, as well as amplifying net evaporation in arid regions; this is known as the “dry gets drier, wet gets wetter” paradigm. According to this paradigm, dry northern China will become drier with global warming, and wet southern China will become wetter. However, Broecker and Putnam (2013) predicted that the Earth’s thermal equator will move northward in a warmer world as continents in the Northern Hemisphere heat up

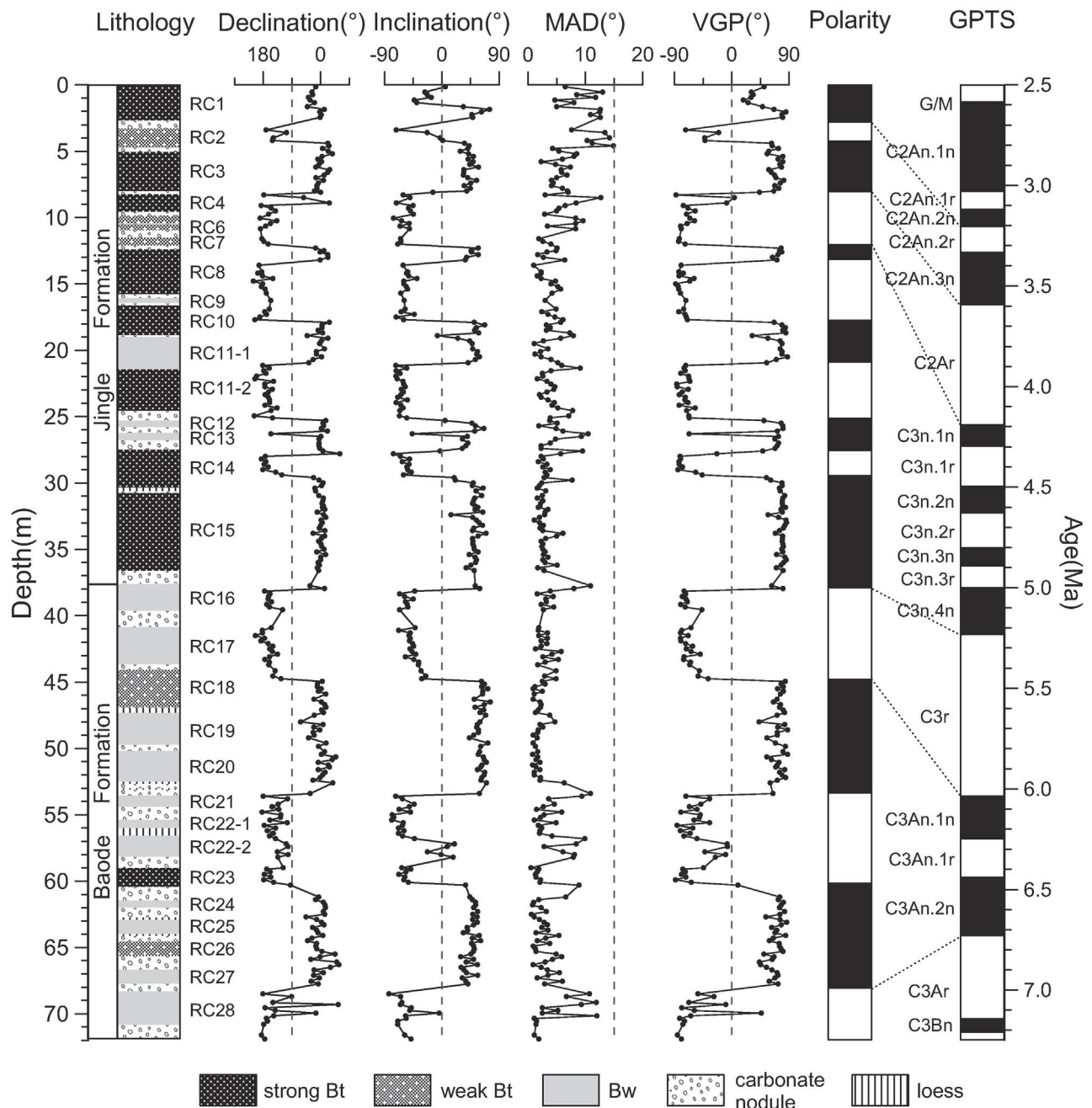


Fig. 4. Lithostratigraphy and magnetic polarity stratigraphy for the Pianguan 'red clay' sequence, and correlation with the geomagnetic polarity time scale (GPTS), after Ogg (2012). MAD is the maximum angular deviation.

more rapidly than the oceans in the Southern Hemisphere, thus leading to a northward shift in the Asian monsoonal rainbelt, and consequently wetter East Asian mid-latitudes.

Our recent study of spatiotemporal changes in  $C_4$  vegetation showed a minimum 300 km northwestward migration of the East Asian monsoonal rainbelt from the Last Glacial Maximum (LGM) to the mid-Holocene (Yang et al., 2015a). Our results in this study show a further northward migration of the East Asian monsoonal rainbelt during the Pliocene, particularly during 5.23–4.3 Ma and 3.7–2.9 Ma. These observations strongly support the aforementioned prediction by Broecker and Putnam (2013). The northward shift of Earth's thermal equator during the Pliocene is also supported by the northward shift of the West African Monsoon, as indicated by a smaller Sahara desert and a northward extension of forests, woodlands and savannah into today's arid regions (Salzmann et al., 2008; Vallé et al., 2014).

A distinctive feature of the Pliocene climate was a reduced meridional temperature gradient (Brierley et al., 2009; Fedorov et al., 2013; Haywood et al., 2016), due to a pronounced global warming, accentuated at high latitudes (up to  $\sim 19^\circ\text{C}$  warmer than the present day), which has been confirmed by paleotemperature reconstructions based on plant and animal remains and other proxies in the geological records from northern high latitudes (Tedford and Harington, 2003; Ballantyne et al., 2010; Csank et al., 2011). The high-latitude warmth in the Pliocene could be explained by elevated  $\text{CO}_2$  and reduced high-latitude terrestrial ice sheets and sea-ice cover, and associated ice-albedo feedbacks (Haywood and Valdes, 2004; Lunt et al., 2012; Hill et al., 2014). Some researchers have suggested that the Pliocene warm interval was also characterized by a substantially reduced zonal sea surface temperature gradient in the equatorial Pacific, i.e. permanent El Niño-like conditions (Wara et al., 2005; Fedorov et al., 2006, 2013; Brierley et al.,

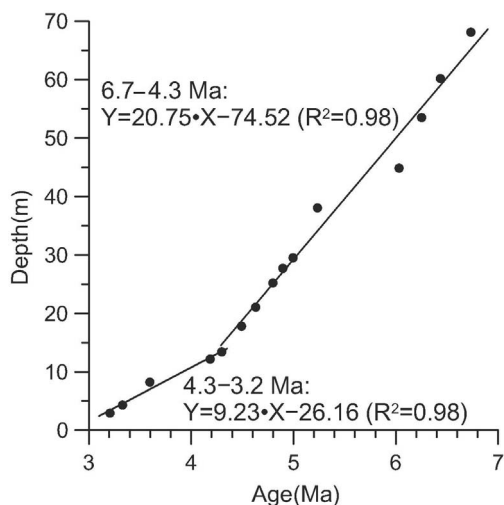


Fig. 5. Age-depth plot for the Pianguan ‘red clay’ sequence. The solid lines are linear regressions for the periods 6.7–4.3 Ma and 4.3–3.2 Ma.

2009). Meteorological observations indicate that the Earth’s thermal equator migrates southward during El Niño events relative to La Niña events (Schneider et al., 2014), resulting in a southward retreat of the EASM rainbelt, with more periods of drought in northern China countered by more floods in southern China (Yang and Lau, 2004).

Conversely, our results show a northward advance of the EASM and humid northern China during Pliocene warmth, consistent with the results from other ‘red clay’ sections across the CLP (Ding et al., 1999, 2001a; He et al., 2013). Therefore, the Pliocene was unlikely to be characterized by a permanent El Niño-like state, but was possibly influenced by a La Niña-like state, a hypothesis which is in agreement with the sea surface temperature record in the equatorial Pacific reconstructed from Mg/Ca measurements of planktonic foraminifera (Rickaby and Halloran, 2005). In this context, we predict that global warming would shift the East Asian climate into a La Niña-like state instead of an El Niño-like state, a finding which deserves to be tested in future studies.

### 7. Conclusions

Rock magnetic studies, including temperature-dependent magnetic susceptibility ( $\chi$ -T), hysteresis loops, IRM acquisition and its back-filed demagnetization measurements, indicate that magnetite of pseudo-single domain size is the dominant remanence carrier in the Pianguan ‘red clay’ sequence. Progressive thermal demagnetization of the ‘red clay’ samples yielded well-defined polarity zones, which are constrained by the age of the Jingle-Baode Formation boundary to be subchrons C2An.2r–C3An.2n, suggesting an age range of 6.9–2.9 Ma for the measured Pianguan section.

The EASM strengthened during two substantive periods, i.e. 5.23–4.3 Ma and 3.7–2.9 Ma, as evidenced by the strong pedogenic

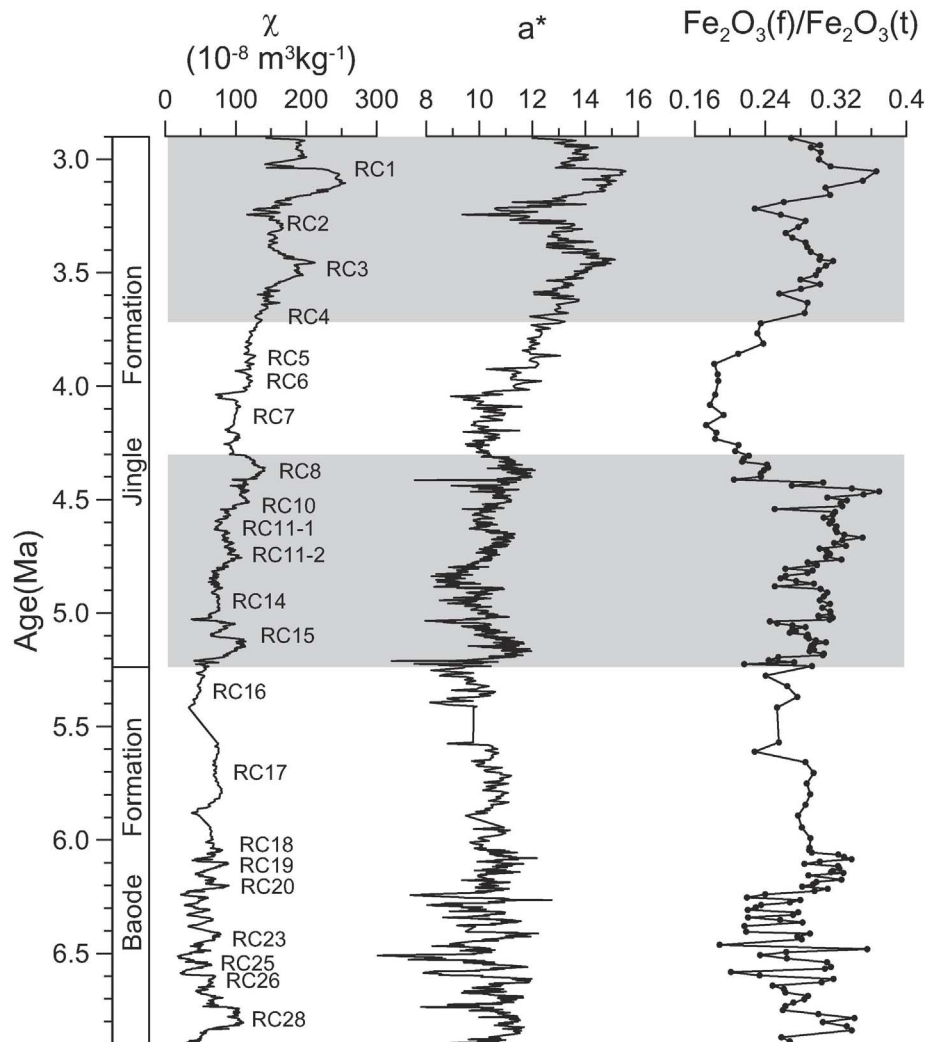


Fig. 6. Changes in magnetic susceptibility ( $\chi$ ), redness ( $a^*$ ), and the ratio of free iron ( $Fe_2O_3(f)$ ) to total iron ( $Fe_2O_3(t)$ ) content of the Pianguan ‘red clay’ sequence for the period 6.9–2.9 Ma. The shaded zones indicate periods characterized by a strengthened East Asian Summer Monsoon.

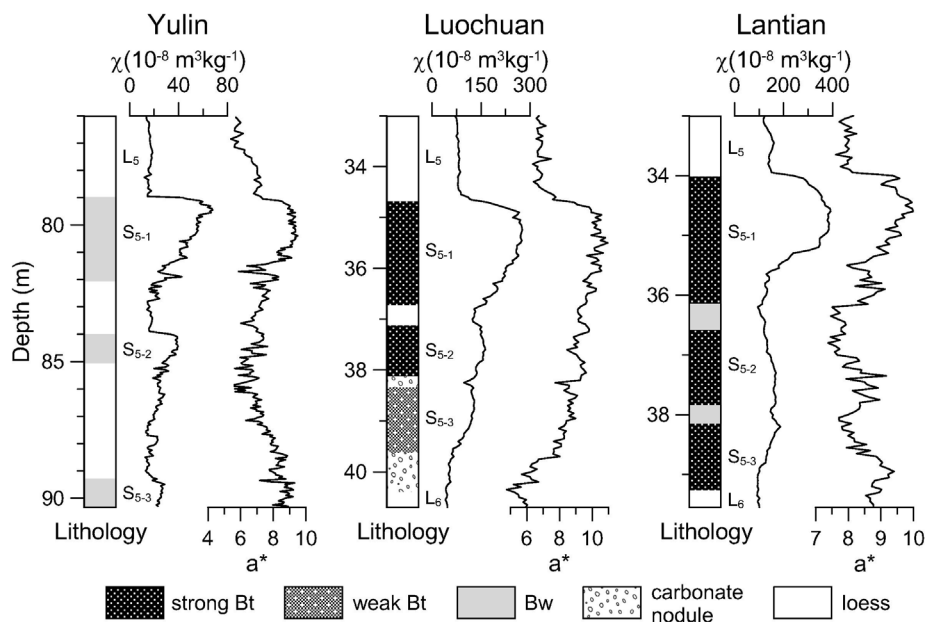


Fig. 7. Lithology, magnetic susceptibility ( $\chi$ ), and redness ( $a^*$ ) records of the paleosol unit  $S_5$  along a north-south transect (Yulin-Luochuan-Lantian).

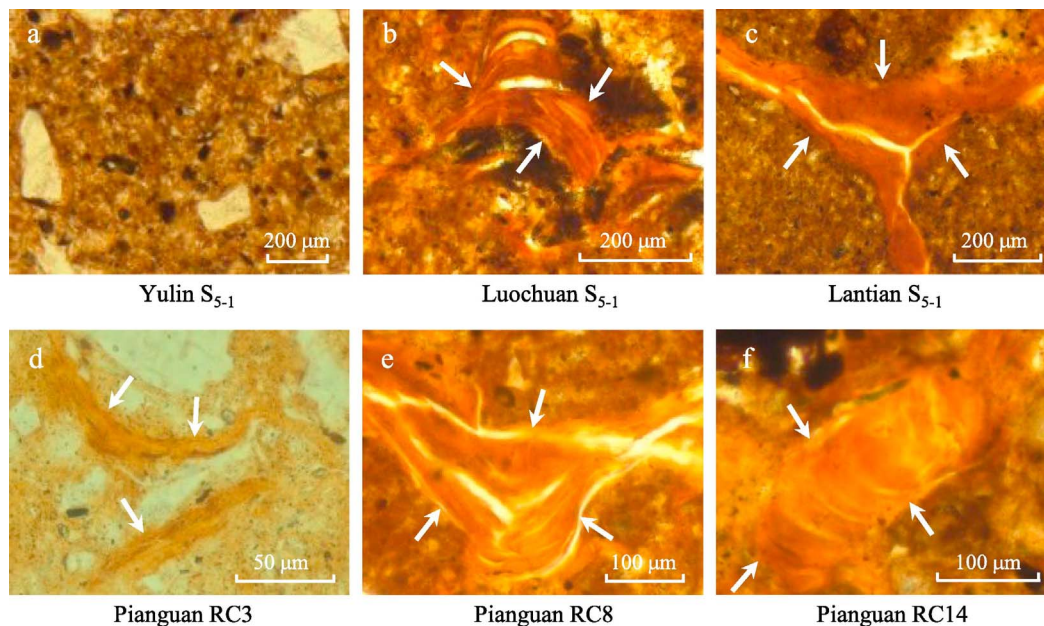


Fig. 8. Thin section photomicrographs (plain-polarized light) of micromorphological samples from the  $S_{5-1}$  paleosol unit along a north-south loess transect (a–c) and across the Pianguan ‘red clay’ sequence (d–f). (a) Micromorphological features of the  $S_{5-1}$  paleosol unit at Yulin, showing sand-sized particles within a silty matrix, and no clay coatings observed. (b) Microlaminated clay coatings in the  $S_{5-1}$  paleosol unit at Luochuan. (c) Thick clay coatings in the  $S_{5-1}$  paleosol unit at Lantian. (d) Clay coatings in RC3 of the Pianguan ‘red clay’ sequence. (e) Microlaminated clay coatings in RC8 of the Pianguan ‘red clay’ sequence. (f) Microlaminated clay coatings in RC14 of the Pianguan ‘red clay’ sequence. The clay coatings are marked by arrows and exhibit sharp or diffuse extinction in cross-polarized light.

development of soils during these two periods, as well as their high free to total  $\text{Fe}_2\text{O}_3$  ratios and high redness values. The well-weathered Pliocene soils at Pianguan have a pedogenic development much stronger than that of the  $S_5$  unit in the northern part of the CLP, but similar to the  $S_5$  unit in the central CLP, indicating a  $\sim 400$  km northward migration of the monsoonal rainbelt during Pliocene warmth compared with the Pleistocene interglacial period ( $\sim 0.5$  Ma ago). This strongly supports the prediction that the Earth’s thermal equator will move northward with global warming. Therefore, we suggest that the semi-arid region in northern China will eventually become wet in a high- $p\text{CO}_2$  world. In addition, our results show that the Pliocene warmth was unlikely to have been characterized by a permanent El Niño-like state, but was possibly influenced by a La Niña-like state.

#### Acknowledgements

This study was supported by the ‘‘Strategic Priority Research Program’’ of the Chinese Academy of Sciences (Grant XDPB0503), the National Key R&D Program of China (Grant 2017YFA0603403), and the National Natural Science Foundation of China (Grants 41672175, 41472318 and 41725010). We thank H.C. Jiang for assistance in the field, G.Q. Chu for laboratory assistance, and J.T. Han and J.A. Mason for valuable discussions and suggestions. We are grateful to two anonymous reviewers for their constructive comments.

## References

- An, Z., 2000. The history and variability of the East Asian paleomonsoon climate. *Quat. Sci. Rev.* 19, 171–187.
- Andersson, J.G., 1923. Essays on the Cenozoic of Northern China. *Mem. Geol. Surv. China Ser. A* 3, 1–152.
- Anwar, T., Kravchinsky, V.A., Zhang, R., 2015. Magneto- and cyclostratigraphy in the red clay sequence: new age model and paleoclimatic implication for the eastern Chinese Loess Plateau. *J. Geophys. Res. Solid Earth* 120, 6758–6770.
- Back, L., Russ, K., Liu, Z., Inoue, K., Zhang, J., Otto-Bliesner, B., 2013. Global hydrological cycle response to rapid and slow global warming. *J. Clim.* 26, 8781–8786.
- Ballantyne, A.P., Greenwood, D.R., Sinnighe Damsté, J.S., Csank, A.Z., Eberle, J.J., Rybczynski, N., 2010. Significantly warmer Arctic surface temperatures during the Pliocene indicated by multiple independent proxies. *Geology* 38, 603–606.
- Bartoli, G., Hönisch, B., Zeebe, R.E., 2011. Atmospheric CO<sub>2</sub> decline during the Pliocene intensification of Northern Hemisphere glaciations. *Paleoceanography* 26, PA4213. doi: <http://dx.doi.org/10.1029/2010PA002055>.
- Beerling, D.J., Royer, D.L., 2011. Convergent Cenozoic CO<sub>2</sub> history. *Nat. Geosci.* 4, 418–420.
- Bloemendal, J., King, J.W., Hall, F.R., Doh, S.J., 1992. Rock magnetism of Late Neogene and Pleistocene deep-sea sediments: relationship to sediment source, diagenetic processes, and sediment lithology. *J. Geophys. Res.* 97, 4361–4375.
- Brierley, C.M., Fedorov, A.V., Liu, Z., Herbert, T.D., Lawrence, K.T., LaRiviere, J.P., 2009. Greatly expanded tropical warm pool and weakened Hadley circulation in the early Pliocene. *Science* 323, 1714–1718.
- Broecker, W.S., Putnam, A.E., 2013. Hydrologic impacts of past shifts of Earth's thermal equator offer insight into those to be produced by fossil fuel CO<sub>2</sub>. *Proc. Natl. Acad. Sci. U.S.A.* 110, 16710–16715.
- Cai, M., Wei, M., Xu, D., Miao, Y., Wu, F., Pan, B., 2013. Vegetation and climate changes during three interglacial periods represented in the Luochuan loess-paleosol section, on the Chinese Loess Plateau. *Quat. Int.* 296, 131–140.
- Csank, A.Z., Tripathi, A.K., Patterson, W.P., Eagle, R.A., Rybczynski, N., Ballantyne, A.P., Eiler, J.M., 2011. Estimates of Arctic land surface temperatures during the early Pliocene from two novel proxies. *Earth Planet. Sci. Lett.* 304, 291–299.
- Day, R., Fuller, M., Schmidt, V.A., 1977. Hysteresis properties of titanomagnetites: grain-size and compositional dependence. *Phys. Earth Planet. Inter.* 13, 260–266.
- Ding, Y., 2004. Seasonal march of the East-Asian summer monsoon. In: Chang, C.-P. (Ed.), *East Asian Monsoon*. World Scientific Publishing Co., Pte. Ltd., Singapore, pp. 3–53.
- Ding, Z., Rutter, N., Liu, T., 1993. Pliocene stratigraphy of Chinese loess deposits and climatic cycles in the last 2.5 Myr. *CATENA* 20, 73–91.
- Ding, Z.L., Sun, J.M., Liu, T.S., Zhu, R.X., Yang, S.L., Guo, B., 1998a. Wind-blown origin of the Pliocene red clay formation in the central Loess Plateau, China. *Earth Planet. Sci. Lett.* 161, 135–143.
- Ding, Z.L., Sun, J.M., Yang, S.L., Liu, T.S., 1998b. Preliminary magnetostratigraphy of a thick eolian red clay-loess sequence at Lingtai, the Chinese Loess Plateau. *Geophys. Res. Lett.* 25, 1225–1228.
- Ding, Z.L., Xiong, S.F., Sun, J.M., Yang, S.L., Gu, Z.Y., Liu, T.S., 1999. Pliocene stratigraphy and paleomagnetism of a ~7.0 Ma eolian loess-red clay sequence at Lingtai, Loess Plateau, north-central China and the implications for paleomonsoon evolution. *Palaeogeogr., Palaeoclimatol., Palaeoecol.* 152, 49–66.
- Ding, Z.L., Yang, S.L., Sun, J.M., Liu, T.S., 2001a. Iron geochemistry of loess and red clay deposits in the Chinese Loess Plateau and implications for long-term Asian monsoon evolution in the last 7.0 Ma. *Earth Planet. Sci. Lett.* 185, 99–109.
- Ding, Z.L., Yang, S.L., Hou, S.S., Wang, X., Chen, Z., Liu, T.S., 2001b. Magnetostratigraphy and sedimentology of the Jingchuan red clay section and correlation of the Tertiary eolian red clay sediments of the Chinese Loess Plateau. *J. Geophys. Res.* 106, 6399–6407.
- Dowsett, H.J., Robinson, M.M., Haywood, A.M., Salzmann, U., Hill, D., Sohl, L., Chandler, M., Williams, M., Foley, K., Stoll, D.K., 2010. The PRISM3D paleoenvironmental reconstruction. *Stratigraphy* 7, 123–139.
- Dunlop, D.J., 2002. Theory and application of the Day plot ( $M_{rs}/M_s$  versus  $H_{cr}/H_c$ ) 1. Theoretical curves and tests using titanomagnetite data. *J. Geophys. Res.* 107 (B3), 2056. <http://dx.doi.org/10.1029/2001JB000486>.
- Etheridge, D.M., Steele, L.P., Langenfelds, R.L., Francey, R.J., Barnola, J.M., Morgan, V.I., 1996. Natural and anthropogenic changes in atmospheric CO<sub>2</sub> over the last 1000 years from air in Antarctic ice and firn. *J. Geophys. Res.* 101 (D2), 4115–4128.
- Fedorov, A.V., Dekens, P.S., McCarthy, M., Ravelo, A.C., deMenocal, P.B., Barreiro, M., Pacanowski, R.C., Philander, S.G., 2006. The Pliocene paradox (mechanisms for a permanent El Niño). *Science* 312, 1485–1489.
- Fedorov, A.V., Brierley, C.M., Lawrence, K.T., Liu, Z., Dekens, P.S., Ravelo, A.C., 2013. Patterns and mechanisms of early Pliocene warmth. *Nature* 496, 43–49.
- Han, J., Chen, H., Fyfe, W.S., Guo, Z., Wang, D., Liu, T.S., 2007. Spatial and temporal patterns of grain size and chemical weathering of the Chinese Red Clay Formation and implications for East Asian monsoon evolution. *Geochim. Cosmochim. Acta* 71, 3990–4004.
- Haywood, A.M., Valdes, P.J., 2004. Modelling Pliocene warmth: contribution of atmosphere, oceans and cryosphere. *Earth Planet. Sci. Lett.* 218, 363–377.
- Haywood, A.M., Hill, D.J., Dolan, A.M., Otto-Bliesner, B.L., Bragg, F., Chan, W.L., Chandler, M.A., Contoux, C., Dowsett, H.J., Jost, A., Kamae, Y., Lohmann, G., Lunt, D.J., Abe-Ouchi, A., Pickering, S.J., Ramstein, G., Rosenbloom, N.A., Salzmann, U., Sohl, L., Stepanek, C., Ueda, H., Yan, Q., Zhang, Z., 2013. Large-scale features of Pliocene climate: results from the Pliocene Model Intercomparison Project. *Clim. Past* 9, 191–209.
- Haywood, A.M., Dowsett, H.J., Dolan, A.M., 2016. Integrating geological archives and climate models for the mid-Pliocene warm period. *Nat. Commun.* 7, 10646. <http://dx.doi.org/10.1038/ncomms10646>.
- He, T., Chen, Y., Balsam, W., Qiang, X., Liu, L., Chen, J., Ji, J., 2013. Carbonate leaching processes in the Red Clay Formation, Chinese Loess Plateau: Fingerprinting East Asian summer monsoon variability during the late Miocene and Pliocene. *Geophys. Res. Lett.* 40, 194–198. <http://dx.doi.org/10.1029/2012GL053786>.
- Held, I.M., Soden, B.J., 2006. Robust responses of the hydrological cycle to global warming. *J. Clim.* 19, 5686–5699.
- Heller, F., Liu, T.S., 1982. Magnetostratigraphical dating of loess deposits in China. *Nature* 300, 431–433.
- Heller, F., Liu, T.S., 1984. Magnetism of Chinese loess deposits. *Geophys. J. R. Astr. Soc.* 77, 125–141.
- Heller, F., Liu, X., Liu, T., Xu, T., 1991. Magnetic susceptibility of loess in China. *Earth Planet. Sci. Lett.* 103, 301–310.
- Hill, D.J., Haywood, A.M., Lunt, D.J., Hunter, S.J., Bragg, F.J., Contoux, C., Stepanek, C., Sohl, L., Rosenbloom, N.A., Chan, W.L., Kamae, Y., Zhang, Z., Abe-Ouchi, A., Chandler, M.A., Jost, A., Lohmann, G., Otto-Bliesner, B.L., Ramstein, G., Ueda, H., 2014. Evaluating the dominant components of warming in Pliocene climate simulations. *Clim. Past* 10, 79–90.
- IPCC, 2013. *Climate Change 2013: The Physical Science Basis*. Stocker, T.F., Qin, D., Plattner, G.-K., Tignor, M., Allen, S.K., Boschung, J., Nauels, A., Xia, Y., Bex, V., Midgley, P.M. (Eds.). Cambridge University Press, Cambridge.
- Jiang, W., Cheng, Y., Yang, X., Yang, S., 2013. Chinese Loess Plateau vegetation since the Last Glacial Maximum and its implications for vegetation restoration. *J. Appl. Ecol.* 50, 440–448.
- Jiang, W., Yang, X., Cheng, Y., 2014. Spatial patterns of vegetation and climate on the Chinese Loess Plateau since the Last Glacial Maximum. *Quat. Int.* 334–335, 52–60.
- Kirschvink, J.L., 1980. The least-squares line and plane and the analysis of palaeomagnetic data. *Geophys. J. R. Astr. Soc.* 62, 699–718.
- Levitus, S., Antonov, J.I., Boyer, T.P., Stephens, C., 2000. Warming of the world ocean. *Science* 287, 2225–2229.
- Li, X.R., Fang, X.M., Wu, F.L., Miao, Y.F., 2011. Pollen evidence from Baode of the northern Loess Plateau of China and strong East Asian summer monsoons during the Early Pliocene. *Chinese Sci. Bull.* 56, 64–69.
- Liu, Q., Deng, C., Yu, Y., Torrent, J., Jackson, M.J., Banerjee, S.K., Zhu, R., 2005. Temperature dependence of magnetic susceptibility in an argon environment: implications for pedogenesis of Chinese loess/paleosols. *Geophys. J. Int.* 161, 102–112.
- Liu, Q., Torrent, J., Morrás, H., Ao, H., Jiang, Z., Su, Y., 2010. Superparamagnetism of two modern soils from the northeastern Pampean region, Argentina and its paleoclimatic indications. *Geophys. J. Int.* 183, 695–705.
- Liu, T.S., 1985. *Loess and the Environment*. China Ocean Press, Beijing.
- Liu, X.M., Hesse, P., Rolph, T., 1999. Origin of maghaemite in Chinese loess deposits: aeolian or pedogenic? *Phys. Earth Planet. Inter.* 112, 191–201.
- Liu, X., An, Z., Rolph, T., Qiang, X., Hesse, P., Lu, H., Zhou, J., Cai, Y., 2001. Magnetic properties of the Tertiary red clay from Gansu Province, China and its paleoclimatic significance. *Sci. China (Ser. D)* 44(7), 635–651.
- Lunt, D.J., Haywood, A.M., Schmidt, G.A., Salzmann, U., Valdes, P.J., Dowsett, H.J., Loptson, C.A., 2012. On the causes of mid-Pliocene warmth and polar amplification. *Earth Planet. Sci. Lett.* 321–322, 128–138.
- Lüthi, D., Floch, M.L., Bereiter, B., Blunier, T., Barnola, J.M., Siegenthaler, U., Raynaud, D., Jouzel, J., Fischer, H., Kawamura, K., Stocker, T.F., 2008. High-resolution carbon dioxide concentration record 650,000–800,000 years before present. *Nature* 453, 379–382.
- Maxbauer, D.P., Feinberg, J.M., Fox, D.L., 2016. Magnetic mineral assemblages in soils and paleosols as the basis for paleoprecipitation proxies: a review of magnetic methods and challenges. *Earth Sci. Rev.* 155, 28–48.
- Mehra, O.P., Jackson, M.L., 1960. Iron oxide removal from soils and clays by a dithionite-citrate system buffered with sodium bicarbonate. *Clays Clay Miner.* 7, 317–327.
- Mohtadi, M., Prange, M., Steinke, S., 2016. Paleoclimatic insights into forcing and response of monsoon rainfall. *Nature* 533, 191–199.
- Ogg, J.G., 2012. *Geomagnetic Polarity Time Scale*. In: Gradstein, F.M., Ogg, J.G., Schmitz, M.D., Ogg, G.M. (Eds.), *The Geologic Time Scale 2012*. Elsevier, Amsterdam, pp. 85–113.
- Pagani, M., Liu, Z., LaRiviere, J., Ravelo, A.C., 2010. High Earth-system climate sensitivity determined from Pliocene carbon dioxide concentrations. *Nat. Geosci.* 3, 27–30.
- Passley, B.H., Ayliffe, L.K., Kaakinen, A., Zhang, Z., Eronen, J.T., Zhu, Y., Zhou, L., Cerling, T.E., Fortliak, M., 2009. Strengthened East Asian summer monsoons during a period of high-latitude warmth? Isotopic evidence from Mio-Pliocene fossil mammals and soil carbonates from northern China. *Earth Planet. Sci. Lett.* 277, 443–452.
- Ploeger, F., Günther, G., Konopka, P., Fueglistaler, S., Müller, R., Hoppe, C., Kunz, A., Spang, R., Groß, J.U., Riese, M., 2013. Horizontal water vapor transport in the lower stratosphere from subtropics to high latitudes during boreal summer. *J. Geophys. Res.* Atmos. 118, 8111–8127.
- Qiang, X., An, Z., Li, H., Chang, H., Song, Y., 2005. Magnetic properties of Jiaxin red clay sequences from northern Chinese Loess Plateau and its paleoclimatic significance. *Sci. China, Ser. D Earth Sci.* 48 (8), 1234–1245.
- Quade, J., Broecker, W.S., 2009. Dryland hydrology in a warmer world: Lessons from the Last Glacial period. *Eur. Phys. J. Special Topics* 176 (1), 21–36.
- Rickaby, R.E.M., Halloran, P., 2005. Cool La Niña during the warmth of the Pliocene? *Science* 307, 1948–1952.
- Rogelj, J., den Elzen, M., Höhne, N., Fransen, T., Fekete, H., Winkler, H., Schaeffer, R., Sha, F., Riahi, K., Meinshausen, M., 2016. Paris Agreement climate proposals need a boost to keep warming well below 2 C. *Nature* 534, 631–639.
- Rutter, N., Ding, Z., Evans, M.E., Wang, Y., 1990. Magnetostratigraphy of the Baoji loess-paleosol section in the north-central China Loess Plateau. *Quat. Int.* 7–8, 97–102.
- Salzmann, U., Haywood, A.M., Lunt, D.J., Valdes, P.J., Hill, D.J., 2008. A new global

- biome reconstruction and data-model comparison for the Middle Pliocene. *Global Ecol. Biogeogr.* 17, 432–447.
- Schneider, T., Bischoff, T., Haug, G.H., 2014. Migrations and dynamics of the intertropical convergence zone. *Nature* 513, 45–53.
- Seki, O., Foster, G.L., Schmidt, D.N., Mackensen, A., Kawamura, K., Pancost, R.D., 2010. Alkenone and boron-based Pliocene  $pCO_2$  records. *Earth Planet. Sci. Lett.* 292, 201–211.
- Soil Survey Staff, 1999. *Soil Taxonomy: A Basic System of Soil Classification for Making and Interpreting Soil Surveys*, second ed. Agriculture Handbook No. 436. United States Department of Agriculture, Natural Resources Conservation Service. U.S. Government Printing Office, Washington, DC.
- Stacey, F.D., Banerjee, S.K., 1974. *The Physical Principles of Rock Magnetism*. Elsevier, New York.
- Stober, J.C., Thompson, R., 1979. An investigation into the source of magnetic minerals in some Finnish lake sediments. *Earth Planet. Sci. Lett.* 45, 464–474.
- Sun, D.H., An, Z.S., Shaw, J., Bloemendal, J., Sun, Y.B., 1998. Magnetostratigraphy and palaeoclimatic significance of Late Tertiary aeolian sequences in the Chinese Loess Plateau. *Geophys. J. Int.* 134, 207–212.
- Tedford, R.H., Harington, C.R., 2003. An Arctic mammal fauna from the Early Pliocene of North America. *Nature* 425, 388–390.
- Teilhard de Chardin, P., Young, C.C., 1930. Preliminary observation on the pre-loessic and post-Ponian Formation in western Shanxi and northern Shenxi. *Mem. Geol. Surv. China Ser. A*(8), 1–54.
- Trenberth, K.E., Dai, A., Rasmussen, R.M., Parsons, D.B., 2003. The changing character of precipitation. *Bull. Amer. Meteor. Soc.* 84, 1205–1217.
- Vallé, F., Dupont, L.M., Leroy, S.A.G., Schefuß, E., Wefer, G., 2014. Pliocene environmental change in West Africa and the onset of strong NE trade winds (ODP Sites 659 and 658). *Palaeogeogr. Palaeoclimatol. Palaeoecol.* 414, 403–414.
- Wara, M.W., Ravelo, A.C., Delaney, M.L., 2005. Permanent El Niño-like conditions during the Pliocene warm period. *Science* 309, 758–761.
- Webster, P.J., Magaña, V.O., Palmer, T.N., Shukla, J., Tomas, R.A., Yanai, M., Yasunari, T., 1998. Monsoons: processes, predictability, and the prospects for prediction. *J. Geophys. Res.* 103 (C7), 14451–14510.
- Wu, F., Fang, X., Ma, Y., Herrmann, M., Mosbrugger, V., An, Z., Miao, Y., 2007. Plio-Quaternary stepwise drying of Asia: evidence from a 3-Ma pollen record from the Chinese Loess Plateau. *Earth Planet. Sci. Lett.* 257, 160–169.
- Yang, F., Lau, K.M., 2004. Trend and variability of China precipitation in spring and summer: linkage to sea-surface temperatures. *Int. J. Climatol.* 24, 1625–1644.
- Yang, S.L., Ding, Z.L., 2003. Color reflectance of Chinese loess and its implications for climate gradient changes during the last two glacial-interglacial cycles. *Geophys. Res. Lett.* 30 (20), 2058. <http://dx.doi.org/10.1029/2003GL018346>.
- Yang, S.L., Ding, Z.L., 2004. Comparison of particle size characteristics of the Tertiary 'red clay' and Pleistocene loess in the Chinese Loess Plateau: implications for origin and sources of the 'red clay'. *Sedimentology* 51, 77–93.
- Yang, S., Ding, Z., 2010. Drastic climatic shift at ~2.8 Ma as recorded in eolian deposits of China and its implications for redefining the Pliocene-Pleistocene boundary. *Quat. Int.* 219, 37–44.
- Yang, S., Ding, Z., Li, Y., Wang, X., Jiang, W., Huang, X., 2015a. Warming-induced northwestward migration of the East Asian monsoon rain belt from the Last Glacial Maximum to the mid-Holocene. *Proc. Natl. Acad. Sci. USA* 112, 13178–13183.
- Yang, X., Jiang, W., Yang, S., Kong, Z., Luo, Y., 2015b. Vegetation and climate changes in the western Chinese Loess Plateau since the Last Glacial Maximum. *Quat. Int.* 372, 58–65.
- Zdansky, O., 1923. Fundorte der Hipparion-Fauna um Pao-Te-Hsien in NW-Shansi. *Bull. Geol. Surv. China* 5, 69–82.
- Zheng, H., An, Z., Shaw, J., 1992. New contributions to Chinese Plio-Pleistocene magnetostratigraphy. *Phys. Earth Planet. Inter.* 70, 146–153.
- Zhu, Y., Zhou, L., Mo, D., Kaakinen, A., Zhang, Z., Fortelius, M., 2008. A new magnetostratigraphic frame work for late Neogene *Hipparion* Red Clay in the eastern Loess Plateau of China. *Palaeogeogr. Palaeoclimatol. Palaeoecol.* 268, 47–57.
- Zijderveld, J.D.A., 1967. A.C. demagnetization of rocks: analysis of results. In: Collinson, D.W., Creer, K.M., Runcorn, S.K. (Eds.), *Methods in Paleomagnetism*. Elsevier, New York, pp. 254–286.